Symmetry and diffusivity of the interstitial hydrogen shallow-donor center in In₂O₃

Philip Weiser,¹ Ying Qin,¹ Weikai Yin,¹ Michael Stavola,^{1,*} W. Beall Fowler,¹ and Lynn Boatner²

¹Department of Physics, Lehigh University, Bethlehem, Pennsylvania 18015, USA

² Oak Ridge National Laboratory (ORNL), Materials Science and Technology Division, Oak Ridge, Tennessee 37831, USA

Abstract

Uniaxial-stress experiments performed for the $3306~cm^{-1}$ vibrational line assigned to the interstitial-hydrogen, shallow-donor center in In_2O_3 reveal its symmetry and transition-moment direction. The defect alignment that can be produced by a [001] stress applied at 165~K is due to a process that is also a hydrogen-diffusion jump, providing a microscopic determination of the diffusion constant for H in In_2O_3 and its mechanism. Our experimental results strongly complement theoretical predictions for the structure and diffusion of the interstitial hydrogen donor center in In_2O_3 .

*michael.stavola@Lehigh.edu

 In_2O_3 doped with Sn is a transparent conducting oxide (TCO) that finds widespread application as a coating for low-emissivity windows and as transparent electrodes for light-emitting diodes, solar cells, and flat-panel displays. In spite of many years of application in electronics technology, mechanisms for the conductivity of In_2O_3 remain controversial. Oxygen vacancies and cation interstitials traditionally have been cited as the causes of unintentional n-type conductivity. However, there is a growing body of work that shows that hydrogen centers in TCOs such as In_2O_3 are important shallow donors. In_2O_3 thin films containing hydrogen show In_2O_3 : Hattractive for solar cell applications. In_2O_3 Muon spin resonance experiments find that implanted muons, whose properties mimic those of hydrogen, form shallow donors in In_2O_3 . And theory predicts that interstitial hydrogen (In_2O_3 is to be controlled and optimized, hydrogen's fundamental properties in this material must be understood.

 In_2O_3 has the cubic bixbyite structure with a conventional unit cell that contains 80 atoms.¹ Ref. 15 provides details regarding the bixbyite structure. IR spectroscopy experiments have determined that H_i^+ is the dominant hydrogen-related shallow donor in In_2O_3 and have assigned an O-H vibrational line at 3306 cm⁻¹ to this defect.¹⁶ The lowest energy structure for H_i^+ [AB₀₁ in Fig. 1(a) using the labeling scheme in Refs. 15 and 16] was predicted to have a quasi-trigonal symmetry,¹⁷ and the structures and energies of three metastable configurations for interstitial hydrogen were also calculated.^{15,16}

In the present paper, the sharp vibrational lines observed for single-crystal specimens of In_2O_3 allow us to make structure-sensitive measurements that are not possible with amorphous films. The perturbation of the vibrational properties of H_i^+ in In_2O_3 created by applying uniaxial stress¹⁸ reveals experimentally the symmetry of H_i^+ , its transition moment direction, and, with the help of theory, the mechanism and activation energy for a hydrogen diffusion jump.

The ln_2O_3 samples used in our experiments were bulk single crystals grown in an air ambient by the flux method at the ORNL.^{19,20} We selected single crystals that were especially large in size (typically bigger than 5 x 5 x 2 mm³) to fabricate samples for the application of uniaxial stress. Laue back-reflection X-ray scattering was used to show that our crystals had {100} faces, making it possible for us to prepare samples with either a [001] or [110] long axis for stress experiments. The as-grown crystals already contained hydrogen and showed the 3306 cm⁻¹ line assigned to H_i .

IR absorption spectra were measured with a Bomem DA.3 Fourier transform spectrometer equipped with a KBr beamsplitter and an InSb detector. Uniaxial stress was applied with a push

rod apparatus that was cooled in a variable-temperature Oxford CF 1204 cryostat. The probing light was polarized with a wire grid polarizer that was placed in the IR beam path after the cryostat.

Two different types of stress experiments have been performed.¹⁸ In the first set of experiments, stress was applied to samples at 4.2 K or 77 K where we have found the H_i⁺ center to be static. The applied stress causes centers oriented along inequivalent directions to have different vibrational frequencies. In this case, the symmetry of the defect and the direction of its transition moment could be determined. In the second set of experiments, stress was applied at elevated temperatures to probe whether the H_i⁺ center is able to reorient.²²

Figure 2 shows spectra for the 3306 cm^{-1} line of the H_i^+ shallow-donor center for In_2O_3 samples with stresses applied along the [001] and [110] directions. The 3306 cm^{-1} line has a full-width-at-half-maximum (FWHM) of $\sim 10 \text{ cm}^{-1}$, making it difficult to determine the positions, widths, and relative intensities of its stress-split components. However, our measured spectra have sufficiently high signal to noise ratio for their second derivatives to be evaluated. Because the overlapping peaks are more easily separated in the second derivatives of the measured spectra, we have fit the second-derivative spectra with sums of second derivatives of Gaussian line shapes as is shown in Fig. 2. From the parameters determined from the fits to the second-derivative spectra, satisfactory line shapes for the original absorbance spectra could also be produced.

The symmetry of the H_i^+ shallow donor can be determined from the number of stress-split components and their relative intensities. The stress data shown in Fig. 2 are consistent with the C_{1h} point group. A defect with C_{1h} symmetry has a primary axis along the <110> direction that is normal to the reflection plane of the center. The transition moment for an electric dipole transition can be oriented along the main symmetry axis or can lie in the reflection plane that is normal to this axis without any restriction imposed by symmetry on the angle θ in this plane. The angle θ is measured with respect to the <001> direction that is perpendicular to the <110> primary axis of the defect.

The shift rates and polarization-dependent intensities of the components of a C_{1h} center are shown in Table I (Ref. 23). Data in Fig. 2 show that for the [001] stress direction, the 3306 cm⁻¹ line is separated into two components, a and b. For the [110] stress direction, three components are resolved. For [110] stress, components f and e_2 in Fig. 2 are seen for the polarization parallel to the stress direction and the (unresolved) components e_1 and g are seen for the polarization perpendicular to the stress. From our data, the parameters in Table I that describe the shifts for the 3306 cm⁻¹ line are $A_1 = 16.8 \pm 1$ cm⁻¹/GPa, $A_2 = -9.9 \pm 1$ cm⁻¹/GPa, $A_3 = -9.9 \pm 1$ cm⁻¹/GPa, $A_4 = -9.9 \pm 1$ cm⁻¹/GPa, $A_5 = -9.9 \pm 1$ cm⁻¹/GPa, A

9.8 \pm 1 cm⁻¹/GPa, and A_4 = 5.1 \pm 1 cm⁻¹/GPa. The angle of the transition moment can be determined from the relative intensities of the stress-split components shown in Fig. 2 and the ratios given in Table I. We find an O-H bond angle of θ = 62° \pm 5°. The [111] direction has an angle θ of 54.7°, so the O-H bonding direction for the 3306 cm⁻¹ center is at an angle just 7° greater than the value for a <111> direction, consistent with both the C_{1h} symmetry found experimentally for the defect and the O-H bonding direction near a <111> axis that was predicted by theory.¹⁷

When stress was applied at elevated temperatures (T > 160 K), the relative intensities of the stress-split components of the 3306 cm $^{-1}$ line were changed due to a stress-induced alignment of the inequivalent components of the C_{1h} center. The alignment produced by [001] stress occurs because the a and b orientations of the H_i^+ center have different ground-state energies under stress. These components are then populated according to their Boltzmann factors if sufficient time is allowed for equilibrium to be established.

The greatest alignment was observed for the [001] direction, so we have focused on the results for this stress direction (Fig. 3). To study the kinetics of the formation of this alignment, a sample was cooled to low temperature (either 4.2 K or 77 K are sufficient) prior to the application of a [001] stress between 260 and 270 MPa. This sample then received a series of anneals, for 15 min each, at successively higher temperatures with the stress maintained. After each anneal, the sample was cooled to low temperature for the measurement of polarized IR spectra.

Figs. 3(a) and (b) show second derivatives of spectra for [001] stress for the perpendicular polarization where both the a and b components can be readily separated. Fig. 3(b) shows that component a was decreased in intensity and component b was increased by annealing under [001] stress at a temperature of 175 K. The second-derivative spectra could be fit with the second derivatives of Gaussian line-shape functions. From these fits, the relative intensities of the b and a components could be determined. The quantity, $R_{\perp}(T)$, is defined to be the ratio of the areas of the b and a components for the perpendicular polarization, $R_{\perp}(T) = I_{\perp,b}(T)/I_{\perp,a}(T)$. Fig. 3(c) shows a plot of $R_{\perp}(T)$ divided by its initial value at low temperature, $R_{\perp,0}$, where reorientation could not occur. Values of $R_{\perp}(T)/R_{\perp,0}$ differing from 1 are due to a stress-induced alignment of the H_i^+ center.

While we could only produce a small change in the relative intensity of the a and b components, the alignment that was observed was highly reproducible (for 2 different samples and over 6 experimental runs) and occurred consistently only for annealing temperatures above 160 K under stress. Furthermore, once stress had been applied to a sample at low

temperature, the only change during an anneal under stress was to cycle the temperature between the low initial temperature and the annealing temperature, making our measured spectra sensitive only to the changes that resulted from the anneal under stress.

Fig. 3(c) shows that an anneal of 15 min at 165 K produced a stress-induced alignment that is approximately 0.5 of the value that can be produced by a 15 min anneal at a higher temperature (i.e., 180 K) where the equilibrium value can be achieved. These results yield a time constant for the alignment of the H_i^+ defect by stress of $r^* = 1.3 \pm 0.3 \times 10^3$ s at 165 K.

Theory provides substantial insight into the interpretation of our results. We have extended the calculations reported in Ref. 16 to study the relationship between different H_i^+ sites and the effect of these sites on H_i^+ and μ_i^* diffusion. These hybrid DFT calculations utilize the CRYSTAL06 code²⁴ with conditions as stated in Ref. 16. The lowest-energy O-H site (AB₀₁) shown in Fig. 1(a) has quasi-trigonal symmetry; the computed O-H direction makes a 16.2° angle with the trigonal axis, displaced towards the [011] direction. This result is consistent with the C_{1h} symmetry and the bonding direction near <111> determined by experiment.

Further analysis of the In_2O_3 structure reveals that this lowest-energy H_i^+ site has an equivalent "partner" on an adjacent O. These two H_i^+ sites are shown schematically in Fig. 1(b). It was noted in Ref. 16 that the metastable sites for H_i^+ are predicted to be at least 0.51 eV above the lowest site. Two of these equivalent 0.51 eV sites [type AB_{02} in Ref. (16)] are near the lowest-energy sites, as shown in Fig. 1(b). The other two metastable sites (AB_{03} and AB_{04}) are predicted to be at least 0.8 eV above the lowest-energy site and are external to the inner region shown in Fig. 1(b).

This situation leads to the following observations: The easiest "hop" of H_i^+ between the two equivalent and adjacent lowest-energy sites will be "back-and-forth"; it will not lead to diffusion. To diffuse, the H_i^+ must hop to a higher-energy AB_{02} site and then relax to an external lowest-energy site. This could involve a jump either to the external 0.51 eV site on the same O, or to one of the two internal 0.51 eV sites shown in Fig. 1(b). While experiment cannot distinguish between these two possibilities, our calculations suggest that the latter will be more favorable. In this case the H_i^+ , after jumping to an internal 0.51 eV site, could then relax as shown in Fig. 1(c) to an external lowest-energy site, and the process could repeat as a two-step diffusion process.

A diffusion jump along the pathway shown in Figs. 1(b) and 1(c) is also a process by which a defect alignment can be produced by stress. An H_i^+ center that contributes to component a in the IR spectrum under [001] stress is converted to an H_i^+ center that contributes to component b. The diffusivity of H_i^+ can be determined from the time constant, τ^* , with which the H_i^+ center

becomes aligned. For the diffusion pathway shown in Figs. 1(b) and 1(c), the diffusivity, D_H , is given by $D_H = d^2/(3\tau_0)$, where τ_0 is the time constant for a jump between specific minimum-energy H_i^+ sites and d is the jump distance.²⁵ Furthermore, the time constant for the production of defect alignment for the C_{1h} , H_i^+ center under [001] stress is $\tau^* = \tau_0/9$ (Ref. 25), giving a diffusivity of $D_H = d^2/(27\tau^*)$. With a jump distance of d = 3.003 Å between the closest minimum-energy H_i^+ sites predicted by theory, the H_i^+ diffusivity is determined to be $D_H(165 \text{ K}) = (2.6\pm0.16)\text{x}10^{-20} \text{ cm}^2/\text{s}$ from our stress-alignment results.

A value of the diffusivity of H_i^+ at 723 K, of $D_H(723K) \approx 5x10^{-9}$ cm²/s, has been estimated previously from a measurement of the H_i^+ indiffusion depth resulting from an annealing treatment in an H_2 ambient.¹⁶ When combined with the diffusivity at 165K reported here, whose value is *more than 10 decades away*, the diffusivity of H_i^+ in In_2O_3 is determined to be,

$$D_{H} = 1.1 \times 10^{-5} \text{ cm}^{2}/\text{s exp}(-0.48 \text{ eV/kT}).$$
 (1)

The activation energy for diffusion found here by experiment is remarkably close to the energy difference predicted by theory between the minimum energy configuration for H_i^+ (AB₀₁) and its next-higher metastable state (AB₀₂) shown in Fig. 1(b). These complementary results reveal the importance of the metastable configuration for H_i^+ with a predicted energy of 0.51 eV in the diffusion pathway for interstitial hydrogen. Furthermore, the activation energy for the diffusion of H_i^+ found here is similar to the Mu₁ to Mu₂ site-change energy found in recent experiments for the case of a muon in In₂O₃ (0.46 eV), suggesting that the motion of the muon involves the same diffusion process studied here.²⁶

The discovery of a stress-induced alignment for the interstitial H_i^+ center has provided an experimental probe of the reorientation of this defect. Furthermore, theory finds that the process by which the 3306 cm⁻¹ center reorients under [001] stress is also a diffusion jump! Therefore, the reorientation kinetics of the 3306 cm⁻¹ center reveal the microscopic process by which H_i^+ diffuses in In_2O_3 and provide an elegant spectroscopic strategy for a determination of its diffusion constant from the time constant for a single hydrogen jump.

The work at L.U. was supported by NSF Grant No. DMR 1160756. M.S. is grateful for support for visits to Dresden from the Humboldt Foundation. Research at the Oak Ridge National Laboratory for one author (L.A.B) was supported by the U.S. Department of Energy, Office of Science, Basic Energy Sciences, Materials Sciences and Engineering Division.

References

- 1. I. Hamberg and C. G. Granqvist, J. Appl. Phys. **60**, R123 (1986).
- 2. S. Lee and D. C. Paine, Appl. Phys. Lett. 102, 052101 (2013).
- 3. J. H. W. De Wit, J. Sol. State Chem. 13, 192 (1975).
- 4. J. H. W. De Wit, G. Van Unen, and M. Lahey, J. Phys. Chem. Solids 38, 819 (1977).
- 5. *Oxide Semiconductors*, edited by B. G. Svensson, S. J. Pearton, and C. Jagadish (Academic Press, San Diego, 2013).
- 6. C. G. Van de Walle, Phys. Rev. Lett. 85, 1012 (2000).
- 7. Ç. Kiliç and A. Zunger, Appl. Phys. Lett. 81, 73 (2002).
- 8. A. Janotti and C. G. Van de Walle, Nature Materials 6, 44 (2006).
- 9. P. D. C. King and T. D. Veal, J. Phys. Condens. Matter 23, 334214 (2011).
- 10. M.D. McCluskey, M. C. Tarun, and S. T. Teklemichael, J. Mater. Res. 17, 2190 (2012).
- 11. H. Li and J. Robertson, J. Appl. Phys. **115**, 203708 (2014).
- 12. T. Koida, H. Fujiwara, and M. Kondo, Jpn. J. Appl. Phys. 46, L685 (2007).
- 13. T. Koida, H. Sai, and M. Kondo, Thin Solid Films 11, 2930 (2010).
- 14. P. D. C. King, R. L. Lichti, Y. G. Celebi, J. M. Gil, R. C. Vilão, H. V. Alberto, J. Piroto Duarte, D. J. Payne, R. G. Egdell, I. McKenzie, C. F. McConville, S. F. J. Cox, and T. D. Veal, Phys. Rev. B 80, 081201(R) (2009).
- 15. S. Limpijumnong, P. Reunchan, A. Janotti, and C. G. Van de Walle, Phys. Rev. B **80**, 193202 (2009).
- 16. W. Yin, K. Smithe, P. Weiser, M. Stavola, W. B. Fowler, L. Boatner, S. J. Pearton, D. C. Hays, and S. Koch, Phys. Rev. B **91**, 075208 (2015).
- 17. W. B. Fowler, M. Stavola, and F. Beklisi, AIP Conf. Proc. **1583**, 359 (2014).
- 18. M. Stavola, in *Identification of Defects in Semiconductors*, edited by M. Stavola (Academic Press, San Diego, 1999), Chap. 3, p. 153.

- 19. J. P. Remeika and E. G. Spencer, J. Appl. Phys. **35**, 2803 (1964).
- D. R. Hagleitner, M. Menhart, P. Jacobson, S. Blomberg, K. Schulte, E. Lundgren, M. Kubicek, J. Fleig, F. Kubel, C. Puls, A. Limbeck, H. Hutter, L. A. Boatner, M. Schmid, and U. Diebold, Phys. Rev. B 85, 115441 (2012).
- 21. J. W. Corbett, R. S. McDonald, and G. D. Watkins, J. Phys. Chem. Solids 25, 873 (1964).
- 22. A. A. Kaplyanskii, Opt. Spectrosc. 16, 329 (1964).
- 23. G. Davies, E. C. Lightowlers, M. Stavola, K. Bergman, and B. Svensson, Phys. Rev. B **35**, 2755 (1987).
- 24. R. Dovesi, V. R. Saunders, C. Roetti, R. Orlando, C. M. Zicovich-Wilson, F. Pascale, B. Civalleri, K. Doll, N. M. Harrison, I. J. Bush, Ph. D'Arco, M. Llunell, *Crystal06 User's Manual*, University of Torino, Torino, 2006.
- 25. A. S. Nowick and B. S. Berry, *Anelastic Relaxation in Crystalline Solids* (Academic Press, New York, 1972).
- 26. These calculations have been extended to consider the diffusion of μ_i* as reported in, B. B. Baker, Y. G. Celebi, R. L. Lichti, P. W. Mengyan, and E. Catak, AIP Conf. Proc. **1583**, 323 (2014). Here we find that the low mass of the μ_i* causes it to be delocalized and shared by the pair of lowest-energy sites shown in Fig. 1(b). Its diffusion will most likely proceed by thermal excitation to a state shared by the pair of higher-energy states shown in Fig. 1(b), after which it will leave the internal region and repeat the process.

Table I. Uniaxial stress perturbations for a C_{1h} center for the [001] and [110] stress directions, with viewing directions along [100] and [001], respectively. The column on the right-hand side gives the theoretical results for the relative intensities of the stress-split absorption lines for a specific angle θ of the transition moment.

stress	component	shift rate	E//001 : E//010
[001]	а	A ₁	$4(\cos^2\theta)$: $2(\sin^2\theta)$
	b	A_2	$4(\sin^2\theta):2(\cos^2\theta+1)$
			E //110: E //110
[110]	e ₁	$(A_1+A_2)/2-A_4$	$(2^{1/2}\cos\theta-\sin\theta)^2:(2^{1/2}\cos\theta+\sin\theta)^2$
	e_2	$(A_1+A_2)/2+A_4$	$(2^{1/2}\cos\theta+\sin\theta)^2:(2^{1/2}\cos\theta-\sin\theta)^2$
	f	A_2 - A_3	$2(\sin^2\theta):0$
	g	$A_2 + A_3$	0 : 2(sin²θ)

Figure captions

FIG. 1. (Color online) (a) The lowest energy antibonding configuration (AB₀₁) for H_i⁺ in In₂O₃. (b) The two red (lower) H_i⁺ sites in In₂O₃ of type AB₀₁ with minimum energy. The two green (upper) hydrogen sites are metastable configurations of type AB₀₂ with predicted energies 0.51 eV higher than AB₀₁. (c) An AB₀₁ site external to the region shown in (b). This was constructed by MOLDRAW (P. Ugliengo, Torino 2006, available at http://www.moldraw.unito.it) and POV-Ray (http://povray.org).

FIG. 2. (Color online) Effect of stress σ applied at T = 6 K along the [001] and [110] directions for the 3306 cm⁻¹ line of the H_i⁺ center in In₂O₃. IR spectra (resolution 2 cm⁻¹) are shown by the thick solid black lines in the center of each panel. The second derivative of the spectrum (open circles) and its fit (solid line) are shown at the top of each panel. The absorbance spectrum and its stress-split components are shown below the measured spectrum (solid lines).

FIG. 3. (Color online) (a) and (b) show the second derivatives of spectra (resolution 2 cm⁻¹), measured for a [001]-oriented sample at T = 6K (perpendicular polarization), of the 3306 cm⁻¹ line. (a) shows the spectrum for a sample cooled to 6K where a stress of 270 MPa was then applied (black line). The red line in (a) shows the spectrum after a subsequent annealing treatment for which the sample was warmed to 145K for 15 min and then re-cooled back to 6K with the stress maintained. (b) shows results for the same sample, except in this case, the red line shows the spectrum after a subsequent annealing treatment at 175K. (c) The normalized ratio of the intensities of the b to a components, $R_{\perp}(T)/R_{\perp,0}$, vs. the annealing temperature. For some of our experiments, the low temperature where stress was first applied was 6 K (filled data points). For others, 77K was the low temperature where stress was first applied (open data points). The solid line in (c) is a guide to the eye.

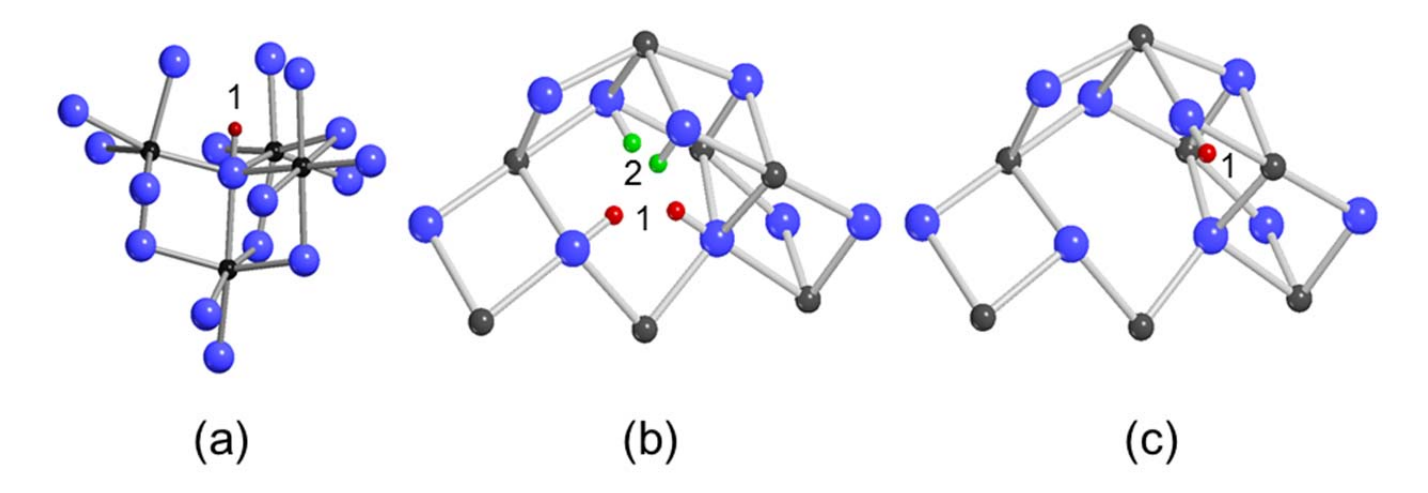


FIG. 1.

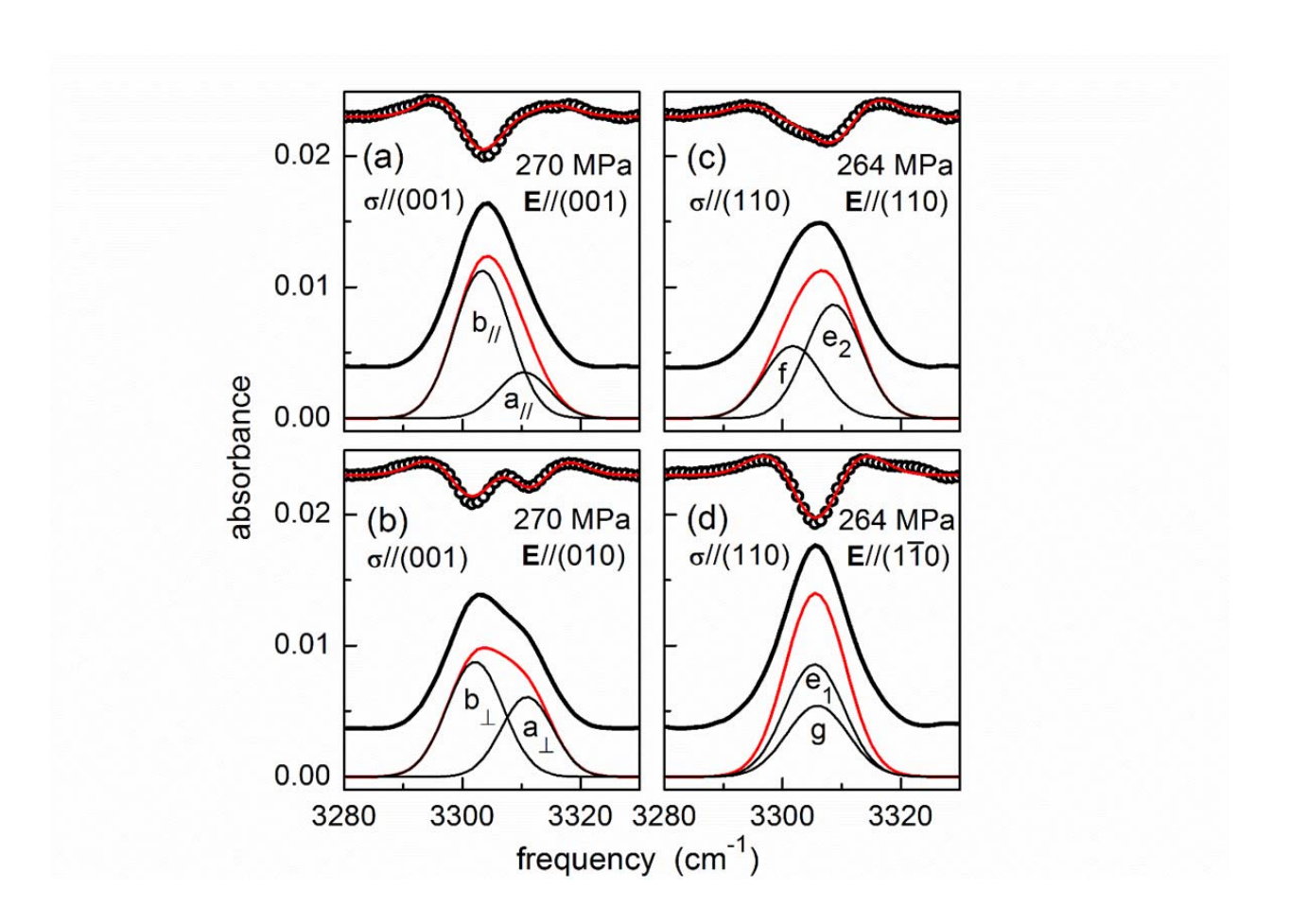


FIG. 2.

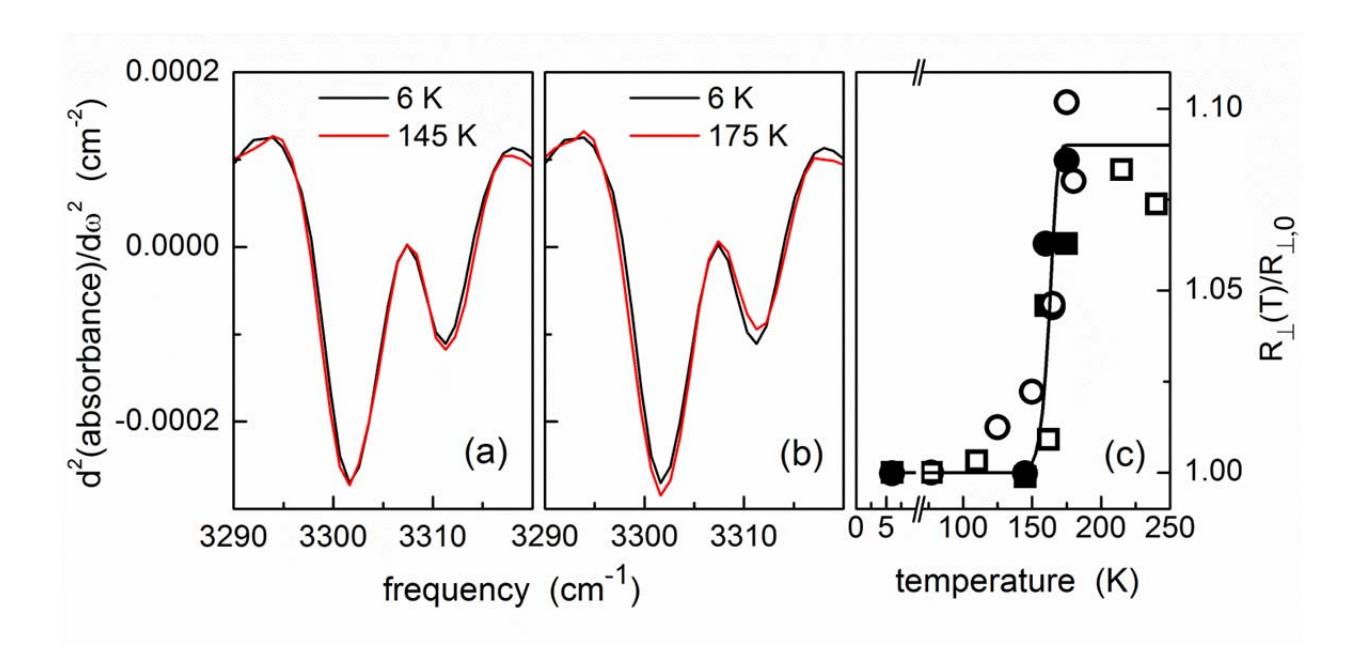


FIG. 3.

